



Kent Academic Repository

Arias-Martorell, Júlia, Urciuoli, Alessandro, Almécija, Sergio, Alba, David M and Nakatsukasa, Masato (2023) *The radial head of the Middle Miocene ape *Nacholapithecus kerioi*: Morphometric affinities, locomotor inferences, and implications for the evolution of the hominoid humeroradial joint.* *Journal of Human Evolution*, 178 . ISSN 0047-2484.

Downloaded from

<https://kar.kent.ac.uk/100710/> The University of Kent's Academic Repository KAR

The version of record is available from

<https://doi.org/10.1016/j.jhevol.2023.103345>

This document version

Author's Accepted Manuscript

DOI for this version

Licence for this version

CC BY-NC-ND (Attribution-NonCommercial-NoDerivatives)

Additional information

Versions of research works

Versions of Record

If this version is the version of record, it is the same as the published version available on the publisher's web site. Cite as the published version.

Author Accepted Manuscripts

If this document is identified as the Author Accepted Manuscript it is the version after peer review but before type setting, copy editing or publisher branding. Cite as Surname, Initial. (Year) 'Title of article'. To be published in **Title of Journal** , Volume and issue numbers [peer-reviewed accepted version]. Available at: DOI or URL (Accessed: date).

Enquiries

If you have questions about this document contact ResearchSupport@kent.ac.uk. Please include the URL of the record in KAR. If you believe that your, or a third party's rights have been compromised through this document please see our [Take Down policy](https://www.kent.ac.uk/guides/kar-the-kent-academic-repository#policies) (available from <https://www.kent.ac.uk/guides/kar-the-kent-academic-repository#policies>).

Short Communication

The radial head of the Middle Miocene ape *Nacholapithecus kerioi*: Morphometric affinities, locomotor inferences, and implications for the evolution of the hominoid humeroradial joint

Julia Arias-Martorell^{a,b,*}, Alessandro Urciuoli^{c,d,a}, Sergio Almécija^{e,f,a}, David M. Alba^a,
Masato Nakatsukasa^g

^a *Institut Català de Paleontologia Miquel Crusafont, Universitat Autònoma de Barcelona, Edifici ICTA-ICP, c/ Columnes s/n, Campus de la UAB, 08193 Cerdanyola del Vallès, Barcelona, Spain*

^b *School of Anthropology and Conservation, Marlowe Building, University of Kent, Canterbury, CT2 7NR, UK*

^c *Universitat Autònoma de Barcelona, Campus de la UAB, 08193 Cerdanyola del Vallès, Barcelona, Spain*

^d *Division of Palaeoanthropology, Senckenberg Research Institute and Natural History Museum Frankfurt, Frankfurt am Main, Germany*

^e *Division of Anthropology, American Museum of Natural History, Central Park West at 79th Street, New York, NY 10024, USA*

^f *New York Consortium in Evolutionary Primatology, New York, NY 10024, USA*

^g *Laboratory of Physical Anthropology, Graduate School of Science, Kyoto University, 606-8502 Kyoto, Japan*

*Corresponding author.

E-mail address: julia.arias@icp.cat (J. Arias-Martorell).

Acknowledgments

We would like to thank NACOSTI for permission to carry out this research in Kenya; we also thank the Director, Head of Earth Sciences and Palaeontology Section Staff at the National Museums of Kenya for their support and collaboration in this project. We would also like to thank the Associate Editor and three reviewers for their help improving earlier versions of this manuscript. This work is part of R+D+I projects PID2020-116908GB-I00 and PID2020-117289GBI00, funded by the Agencia Estatal de Investigación of the Spanish Ministry of Science and Innovation (MCIN/AEI/10.13039/501100011033/). Research has also been supported by the Generalitat de Catalunya/CERCA Programme, the Agència de Gestió d'Ajust Universitaris i de Recerca of the Generalitat de Catalunya (2022 SGR 01188 and 2022 SGR 00620, and Beatriu de Pinós Programme—H2020 MSCA-Cofund Grant No 801370 to J.A.M), a Margarita Salas postdoctoral fellowship funded by the European Union-NextGenerationEU to A.U, and the grants JPJSBP120216301 and KAKENHI 22H02708 to M.N.

1 **Short Communication**

2 The radial head of the Middle Miocene ape *Nacholapithecus kerioi*: Morphometric affinities,
3 locomotor inferences, and implications for the evolution of the hominoid humeroradial joint

4

5 Keywords: Miocene apes; Forelimb; Elbow joint; Pronosupination; Locomotion; 3D

6 geometric morphometrics

7

8

9 1. Introduction

10 The systematic position of the Middle Miocene large-bodied ape *Nacholapithecus*
11 *kerioi* (see review in Nakatsukasa and Kunimatsu, 2009) is somewhat uncertain (e.g.,
12 Almécija et al., 2021), being considered a stem hominid by some researchers (Alba, 2012;
13 Kunimatsu et al., 2019) but being favored as a stem hominoid by recent cladistic analyses
14 (Pugh, 2022). The remains of this species, dated to the Middle Miocene (16 –15 Ma; Sawada
15 et al., 1998, 2006; Nakatsukasa and Kunimatsu, 2009), were originally discovered in the Aka
16 Aiteputh Formation of the Nachola region (northern Kenya) and assigned to *Kenyapithecus*
17 (Ishida et al., 1984; Rose et al., 1996; Nakatsukasa et al., 1998). However, the discovery of
18 the articulated partial skeleton KNM-BG 35250, of which numerous postcranial elements and
19 the cranium were recovered (Nakatsukasa et al., 1998; Ishida et al., 2004), prompted the
20 description of a new genus and species for the large-bodied hominoid from Nachola (Ishida et
21 al., 1999).

22 Many postcranial elements of *N. kerioi* have been described in detail from the
23 holotype KNM-BG 25350 skeleton (Nakatsukasa et al., 1998, 2003a, 2007b, 2012; Ishida et
24 al., 2004; Senut et al., 2004; Kikuchi et al., 2012, 2015, 2016; Ogihara et al., 2016; Takano et
25 al., 2018), as well as from numerous (mostly isolated) finds (Rose et al., 1996; Nakatsukasa et
26 al., 2003b, 2007a; Pina et al., 2021; Takano et al., 2020). From these studies, it has been
27 inferred that *N. kerioi* possessed a pronograde body plan (narrow thorax, long and flexible
28 vertebral column, and limbs used mostly in the parasagittal plane; Nakatsukasa and
29 Kunimatsu, 2009), like other Early and Middle Miocene apes such as *Ekembo* and *Equatorius*
30 (see review in Ward, 2015). However, *Nacholapithecus* exhibits derived postcranial features
31 compared with those of earlier (e.g., *Ekembo*) and contemporaneous (e.g., *Equatorius*) stem
32 hominoids, especially in the elbow joint, which exhibits a deep zona conoidea and a large,
33 globular, and medially tilted capitulum in the distal humerus (Nakatsukasa and Kunimatsu,
34 2009; Takano et al. 2020). These derived features indicate that *Nacholapithecus* displays the

35 earliest known evidence of increased forelimb-dominated behaviors with enhanced vertical
36 climbing capabilities among fossil apes (Nakatsukasa and Kunimatsu, 2009; Takano et al.,
37 2018, 2020).

38 The distal humeral and proximal ulnar morphology of *Nacholapithecus* have been
39 interpreted from a locomotor viewpoint (Takano et al., 2018, 2020) but its proximal radial
40 morphology remains to be analyzed from this perspective. The distinctively derived proximal
41 radial morphology of extant hominoids is functionally related to wide ranges of
42 pronosupination coupled with universal stability at the humeroradial joint (Sarmiento, 1988;
43 Rose, 1988, 1993; Sarmiento et al., 2002: Fig. 4) and has been used to make locomotor
44 inferences in fossil catarrhines (Arias-Martorell et al., 2021). Therefore, here we provide a
45 quantitative morphological analysis of the radial head of *N. kerioi* with the objective of
46 refining previous locomotor inferences for this species. Our analysis is based on the isolated
47 proximal radius fragment KNM-BG 40021 from the fossiliferous site BG-K (see Takano et
48 al., 2020 for a full description of the specimen). We compare it with stem catarrhines and
49 other Miocene hominoids by means of three-dimensional geometric morphometrics (3DGM)
50 to establish its closest morphometric affinities.

51

52 **2. Materials and methods**

53 *2.1. Studied and comparative sample*

54 The right proximal radial fragment of *N. kerioi* KNM-BG 40021 (Fig. 1; Takano et al.,
55 2020) is housed at the National Museums of Kenya (KNM, Nairobi, Kenya). KNM-BG 40021
56 is a 63 mm-long fragment preserving the radial head, radial tuberosity, and a small section of
57 the shaft below the radial tuberosity. The specimen has compression damage affecting mainly
58 the shaft and radial tuberosity, which are both flattened anteroposteriorly. The posterior aspect
59 of the radial head is also flattened, affecting the depth of the fovea, which shows an
60 artifactually increased depth. However, the anterior and medial/lateral aspects of the radial

61 head are well-preserved and preserve their original morphology, including the outline of the
62 fovea (Takano et al., 2020). Our analyses focused on this undistorted and well-preserved
63 aspect of the radial head, the shape of which we characterized using 3DGM to capture more
64 subtle aspects of variation such as the curvature and outline of the radial head, which are very
65 important aspects of radial head variation and function.

66 The comparative fossil sample includes 3D virtual models of the radii of the
67 dendropithecids *Simiolus enjisessi* and *Dendropithecus macinessi*, the pliopithecoid
68 *Epipliopithecus vindobonensis*, and the stem hominoids *Ekembo heseloni* and *Equatorius*
69 *africanus* (see Supplementary Online Material [SOM] Table S1 for further details). The
70 extant comparative sample is the same as in Arias-Martorell et al. (2021), including 116 radii
71 from 26 anthropoid species including all extant hominoid genera (SOM Table S2). Three-
72 dimensional landmarks were collected from 3D models of the radii listed in SOM Tables S1
73 and S2. Details about the scanning procedures of both the fossil and extant comparative
74 sample are presented in SOM S1 and SOM Table S2. All 3D models from right radii
75 (including fossils) were mirrored to the left side during the process of mesh reconstruction as
76 most extant anthropoid radii in our sample are from the left side. Landmarks were placed
77 using IDAV Landmark Editor v. 3.6 (Wiley et al., 2005) and all statistical analysis were done
78 with the statistical environment R v. 4.1.1 (R Core Team, 2021).

79

80 2.2. Geometric morphometric analyses

81 The shape affinities of KNM-BG 40021 were explored using a landmark protocol
82 specifically designed to capture the most informative aspects of shape preserved in this
83 specimen (Fig. 2; for further details see SOM S1 and Table S3). We performed a generalized
84 Procrustes analysis (GPA) with the ‘Morpho’ v. 2.8 package (Schlager, 2017) in R (R Core
85 Team, 2021). We applied semilandmark sliding (identified with SMvector; Schlager, 2017)
86 on curves defined by adjacent landmarks and identified with the function ‘outline’ (Schlager,

87 2017). To identify major patterns of shape variation across the sample, we performed a
88 between-group principal component analysis (bgPCA; Mitteroecker and Bookstein, 2011) on
89 the GPA-transformed coordinates of the extant sample, with major anthropoid clades
90 (platyrrhines, cercopithecines, colobines, hylobatids, and hominids) as the grouping factor. To
91 rule out the presence of spurious groupings in the sample, we computed a cross-validated
92 bgPCA and compared the results to those of the bgPCA without cross-validation (Bookstein,
93 2019; Cardini et al., 2019; Cardini and Polly, 2020). We computed the Z scores and r^2 for
94 group differences in the raw shape data (Adams and Collyer, 2016), and the scores of both the
95 non-cross-validated and the cross-validated bgPCAs using the ‘RRPP’ v. 2.5 R package
96 (Collyer and Adams, 2018; SOM S1). The fossils were left ungrouped and plotted a posteriori
97 onto the morphospace identified by the bgPCA based on extant taxa. To assess the affinities
98 of each fossil specimen with the a priori defined groups we computed the squared
99 Mahalanobis distances between each individual and the group means using the D2.dist
100 function of the ‘biotools’ v. 4.2 (Da Silva, 2020) R package, as well as their typicality
101 probabilities using the function typprobClass in ‘Morpho’ (Table 1; SOM S1). To visualize
102 shape changes occurring along the bgPC axes, we identified the extreme landmark
103 conformations for each bgPC and then warped the 3D model of the individual closest to the
104 mean configuration of the sample—identified with the function ‘FindMeanSpec’ within
105 ‘geomorph’ v. 3.1.1 R package (Adams et al., 2020)—toward the obtained configurations. We
106 finally computed an unweighted pair group methods with arithmetic mean (UPGMA) cluster
107 analysis (SOM S1).

108 To assess correlations between size and shape, ordinary least squares (OLS) and
109 phylogenetic generalized least squares (PGLS; Adams, 2014) regressions of bgPC scores vs.
110 log-transformed centroid size (CS; with natural logarithms, \ln CS) were computed using the
111 ‘geomorph’ v. 3.1.1 R package (Adams et al., 2020). To compute the PGLS regressions, we
112 used a time-calibrated phylogenetic tree based on molecular data downloaded from 10kTrees

113 website v. 3 (Arnold et al., 2010; SOM S1). To evaluate the influence of phylogeny vs.
114 function on the proximal radial shape among extant anthropoids, phylogenetic signal was also
115 quantified by means of both Pagel's λ and Blomberg's K statistics (Pagel, 1999; Blomberg et
116 al., 2003; see SOM S1 for further details) using the 'phytools' v. 0.6-60 R package (Revell,
117 2012).

118

119 **3. Results**

120 The bgPCA (Fig. 3) discriminates among extant hominids, hylobatids, and monkeys and
121 correctly classifies 80.2% of cases in the five groups defined a priori (platyrrhines,
122 cercopithecines, colobines, hylobatids, and hominids), while the bgPCA with cross-validation
123 (SOM Fig. S1) correctly classifies 72.4% of cases (SOM S1; SOM Tables S4 and S5).
124 Misclassification cases occur mainly among monkeys, whereas hylobatids are correctly
125 classified in 76% of the cases and hominids in 86% (cross-validated bgPCA; SOM Table S5).

126 There is no perceptible change between the bgPCA (Fig. 3) and the cross-validated
127 bgPCA (SOM Fig. S1) plots, and the Z-scores are similar for the raw data (6.9), bgPCA (8.7),
128 and cross-validated bgPCA (8.7), implying a similar strength of morphological integration in
129 the datasets. Similarly, r^2 increases from the raw data comparisons (0.26) to both standard (0.52)
130 and cross-validated (0.52) bgPCAs. This indicates that grouping structure is not spurious
131 because there is a comparable increase in r^2 from the raw data to both the standard and cross-
132 validated bgPCAs. Only bgPC1 and bgPC2 (which account for 90% of the variance) are
133 discussed below because bgPC3 (7% variance) and bgPC4 (3% variance) yielded no
134 meaningful patterns.

135 The bgPC1 (78% of variance) embeds significant but low phylogenetic signal ($K =$
136 0.35 , $p = 0.027$; $\lambda = 0.54$, $p = 0.016$), suggesting a considerable amount of homoplasy, best
137 illustrated by the overlap between *Ateles* and hominids—see SOM S1 for the different
138 implications of K and λ . Although bgPC1 is significantly correlated with ln CS (OLS: $p <$

139 0.001; PGLS: $p = 0.008$), size only accounts for a small amount of shape variation (OLS: $r^2 =$
140 0.10 and adjusted $r^2 = 0.09$; PGLS: $r^2 = 0.26$ and adjusted $r^2 = 0.23$). This axis discriminates
141 between hominoids (hominids and hylobatids, overlapping toward negative scores) and
142 cercopithecoids and platyrrhines (which mostly display positive scores, particularly
143 colobines)—except for *Ateles*, which mostly overlaps with hominoids (Fig. 3).
144 *Nacholapithecus* displays slightly positive scores within the hominid variation range, whereas
145 all the other fossils, including *Ekembo* and *Equatorius*, fall within the cercopithecoid–
146 platyrrhine distribution (albeit occupying different positions along bgPC1) apart from
147 hominoids. *Simiolus* displays the most positive scores and *Ekembo* is closer to hominoids (but
148 well distinct from *Nacholapithecus*) among the remaining fossil sample. Shape differences
149 along bgPC1 are driven by the shape of the radial head (Fig. 3) and the mediolateral tilting of
150 the head. Stem catarrhines and monkeys other than *Ateles* (more positive scores) display a
151 more elliptic radial head in proximal view and a medial elevation of the head in anterior view,
152 which results into a mediolateral tilting of the head. In contrast, extant hominoids and *Ateles*
153 (more negative scores) have rounder heads that are not tilted (Fig. 3).

154 bgPC2 (12% of variance) embeds no significant phylogenetic signal ($K = 0.22$, $p =$
155 0.312; $\lambda < 0.001$, $p = 1.000$) and is not correlated with ln CS (OLS: $p = 0.083$; PGLS: $p =$
156 0.274). bgPC2 distinguishes between hominids (positive and slightly negative scores) and
157 hylobatids (more negative scores) with some overlap, but both groups largely overlap with
158 cercopithecoids and platyrrhines, which are not distinguished along this axis (Fig. 3). All the
159 fossils analyzed cluster close to one another, with *Nacholapithecus*, *Ekembo*, and
160 *Dendropithecus* displaying scores closer to 0, and *Simiolus* and *Equatorius* displaying slightly
161 negative scores. Shape differences along bgPC2 are also driven by tilting of the head toward
162 more positive scores. More subtle differences include a more uniformly expanded distal
163 surface area of the radial head toward positive scores, whereas in specimens with more

164 negative scores the distally expanded surface area is more restricted to the anteromedial
165 aspect of the head.

166 Based on the typicality probabilities for the fossils (Table 1), *Nacholapithecus* is
167 classified as a platyrrhine as first option and as a hominid as second option. *Ekembo*,
168 *Equatorius*, and *Dendropithecus* are also classified as platyrrhines, whereas *Epipliopithecus*
169 and the two *Simiolus* specimens are classified as cercopithecines. The UPGMA analysis
170 clusters *Nacholapithecus* with a subcluster including all extant hominoids (SOM S2; SOM
171 Fig. S2).

172

173 **4. Discussion and conclusions**

174 We used a landmark protocol that characterizes the anterior aspect of the radial head to
175 analyze the single proximal radial fragment available for *Nacholapithecus*. The overall results
176 are similar to those previously found using a protocol with a more complete proximal radius
177 coverage (Arias-Martorell et al., 2021) but have more limited explanatory power at the
178 morphofunctional level. The shape of the anterior aspect of the radial head is only partially
179 explained by phylogeny, with bgPC2 showing no meaningful phylogenetic signal (as the
180 monkey variation encompasses that of extant hominoids) and bgPC1 displaying significant
181 but low values. The latter denote homoplasy, which might be explained by *Ateles* partially
182 overlapping with hominids due to its convergently evolved hominoid-like humeroradial joint
183 shape (Larson, 1998; Arias-Martorell et al., 2021). Similarities include a round radial head
184 and a more uniform surface area in the distal expansion of the radial head (not circumscribed
185 to the anteromedial side) than in other monkeys (Arias-Martorell et al., 2021).

186 Functional inferences for the elbow complex of *Nacholapithecus* have been based
187 mostly on the forelimb evidence from the holotype (KNM-BG 35250; Ishida et al., 2004;
188 Nakatsukasa and Kunimatsu, 2009; Takano et al., 2018). The modern hominoid-like globular
189 capitulum of the humerus (KNM-BG 35250M) indicates enhanced mobility at the

190 humeroradial joint and suggests enhanced forearm pronosupination capabilities because of the
191 inferred rounder radial head compared with cercopithecids and stem Miocene hominoids
192 (Takano et al., 2018). As indicated by our shape analysis, *Nacholapithecus* possesses a fairly
193 circular radial head outline with limited tilting and a distal articular surface uniformly
194 expanded to some extent beyond the anteromedial aspect of the radial head. On the
195 morphospace, KNM-BG 40021 displays an intermediate position between extant hominoids
196 and monkeys, close to hominids and overlapping with *Ateles*. This is further supported by the
197 fact that the analysis classifies *Nacholapithecus* as a platyrrhine (first option, owing to its
198 similarities to *Ateles*) or as a hominid (second option).

199 The anterior aspect of the radial head articulates with the zona conoidea of the
200 humerus in extant apes, whose humeroradial joint is stable throughout all ranges of
201 pronosupination and flexion–extension (Rose, 1988). In contrast, cercopithecoids, have a
202 stable elbow in fully pronated position, where the humeroantebrachial joint achieves a close-
203 packing position (Harrison 1987; Rose, 1988, 1993; Alba et al., 2011). The more extant
204 hominoid-like and atelid-like anterior aspect of the radial head of *Nacholapithecus* is
205 consistent with a radial head that is able to articulate with both the humerus and the ulna in
206 pronated and semipronated forearm positions due to incipient beveling of the radial head
207 beyond the lateral lip (Rose et al., 1992; Takano et al., 2018, 2020)—achieved, in
208 *Nacholapithecus*, by a rounder head and a more uniform distal expansion of the articular area
209 of the radial head than in cercopithecoids, nonsuspensory platyrrhines, and both earlier and
210 coeval Miocene apes. Relative to extant hominoids, *Nacholapithecus* displays a more
211 primitive humeroulnar joint that is not capable of full extension due to a long olecranon
212 process (Takano et al., 2020) and further retains primitive traits at the wrist joint (e.g.,
213 ulnocarpal articulation; Ogihara et al., 2016). However, these plesiomorphic features are
214 combined with a humeroradial joint somewhat derived toward the extant hominoid condition
215 than that of early hominoids such as *Ekembo* and *Equatorius* (Takano et al., 2018, 2020). The

216 enhanced stability in wider ranges of pronosupination (especially in semipronated arm
217 positions) of the radiohumeral joint indicated by our results is concordant with previous
218 locomotor inferences for *Nacholapithecus*. Its locomotor repertoire has been described as
219 including forelimb-dominated arboreal behaviors with the forelimbs playing an important role
220 in both body support and overhead positions (Takano et al., 2018, 2020)—i.e., vertical
221 climbing, orthograde clambering, transferring, and bridging in higher frequencies than in
222 Early Miocene apes (e.g., *Ekembo*)—combined with powerful grasping abilities (Ishida et al.,
223 2004; Nakatsukasa et al., 2002, 2007a, 2007b, 2012, 2016; Nakatsukasa and Kunitatsu,
224 2009; Alba et al., 2011; Ogihara et al., 2016; Ward, 2015; Takano et al., 2018, 2020).

225 Nevertheless, our results also suggest that the anterior aspect of the radius is not
226 sufficient to distinguish well among groups of quadrupedal taxa with radial heads most suited
227 to maintaining stability in a flexed-elbow and fully pronated hand posture (Rose, 1988)—as
228 illustrated by the considerable overlap between cercopithecines, colobines, and platyrrhines.
229 The fact that small-bodied stem catarrhines and the stem hominoids *Ekembo* and *Equatorius*
230 occupy the same region of the morphospace indicates similarities in the anterior aspect of the
231 radial head, especially in the distal expansion of its articular surface area. This is not
232 surprising given that a more distally expanded anteromedial articular surface area is part of
233 the ancestral anthropoid morphotype (Rose, 1988, 1993, 1994, 1997; Senut, 1989). In
234 previous analyses based on the proximal radius (Arias-Martorell et al., 2021), *Ekembo* and
235 *Equatorius* displayed a clearly intermediate morphology between extant hominoids and
236 monkeys, rather than closer affinities with monkeys. In our bgPCA plot, *Ekembo* is somewhat
237 closer to extant hominoids than *Equatorius* along bgPC1—consistent with differences in their
238 positional behavior (Ward, 1993, 2015; Ward et al., 1993, 1999; McCrossin et al., 1998; Patel
239 et al., 2009)—albeit less so than *Nacholapithecus*, whose humeroradial joint appears more
240 derived toward the crown hominoid condition (Takano et al., 2018, 2020). Small-bodied stem
241 catarrhines display the radial head morphology characteristic of non-hominoid anthropoids

242 and our results broadly agree with those previously obtained (Arias-Martorell et al., 2021)
243 albeit with lower resolution, especially for taxa with a high quadrupedal component.

244 The mosaic configuration of the elbow joint of *Nacholapithecus*, combining a
245 primitive humeroulnar joint with a quite derived humeroradial joint, supports a stepwise
246 evolution of the anthropoid elbow (Alba et al., 2011, 2015), with extant cercopithecoids and
247 hominoids displaying features derived in opposite directions and stem hominoids displaying
248 mosaic morphologies unlike those of living apes (Alba et al., 2011; Arias-Martorell et al.,
249 2021). The uncertain phylogenetic relationships of *Nacholapithecus* (e.g., Almécija et al.,
250 2021; Urciuoli et al., 2021) hinder to some extent the evolutionary implications of its
251 proximal radial morphology. Nevertheless, the proximal radial morphology of
252 *Nacholapithecus*, more derived than that of *Ekembo* but more primitive than that of crown
253 hominoids, likely reflects an enhancement of pronosupination movements associated with an
254 emphasis on orthograde positional behaviors—compatible with both the stem hominoid
255 (Pugh, 2022) and stem hominid (Alba, 2012; Kunitatsu et al., 2019; Morimoto et al., 2020)
256 status proposed for this taxon. Regardless of its systematic position, the elbow morphology of
257 *Nacholapithecus* suggests that the last common ancestor of crown hominoids displayed a
258 humeroradial joint more primitive than extant hominoids—indicating that the
259 humeroantebrachial complex would have evolved to some extent independently between
260 hylobatids and hominids. The latter notion would be consistent with the independent
261 evolution of orthograde-related features in atelids and various lineages of crown hominoids
262 (Larson, 1998; Alba, 2012; Almécija et al., 2021) and is further reinforced by the retention of
263 primitive features (likely related to above-branch quadrupedalism) in the humeroulnar joint of
264 the Late Miocene great ape *Hispanopithecus*—recovered as a stem hominid by cladistic
265 analyses (Alba et al., 2015; Pugh, 2022)—despite indicating an elbow complex suitable for
266 preserving stability along the full range of flexion/extension and enabling a broad range of
267 pronosupination as in extant hominoids (Alba et al., 2012).

268

269 **References**

270 Adams, D.C., 2014. A method for assessing phylogenetic least squares models for shape and
271 other high-dimensional multivariate data. *Evolution* 68, 2675–2688.

272 Adams, D.C., Collyer, M.L. 2016. On the comparison of the strength of morphological
273 integration across morphometric datasets. *Evolution* 70, 2623–2631.

274 Adams, D.C., Collyer, M.L., Kaliontzopoulou, A., 2020. Geomorph: Software for geometric
275 morphometric analyses. R package version 3.2.1. [https://cran.r-](https://cran.r-project.org/package=geomorph)
276 [project.org/package=geomorph](https://cran.r-project.org/package=geomorph).

277 Alba, D.M., 2012. Fossil apes from the Vallès-Penedès Basin. *Evol. Anthropol.* 21, 254–269.

278 Alba, D.M., Almécija, S., DeMiguel, D., Fortuny, J., Pérez de los Ríos, M., Pina, M., Robles,
279 J.M., Moyà-Solà, S., 2015. Miocene small-bodied ape from Eurasia sheds light on
280 hominoid evolution. *Science* 350, aab2625.

281 Almécija, S., Hammond, A.S., Thompson, N.E., Pugh, K.D., Moyà-Solà, S. Alba, D.M. 2021.
282 Fossil apes and human evolution. *Science* 372, eabb4363.

283 Almécija, S., Smaers, J.B. Jungers, W.L. 2015. The evolution of human and ape hand
284 proportions. *Nat. Comm.* 6, 1–11.

285 Arias-Martorell, J., Almécija, S., Urciuoli, A., Nakatsukasa, M., Moyà-Solà, S., Alba, D.M.
286 2021. A proximal radius of *Barberapithecus huerzeleri* from Castell de Barberà:
287 Implications for locomotor diversity among pliopithecoids. *J. Hum. Evol.* 157, 103032.

288 Arnold, C., Matthews, L.J., Nunn, C.L., 2010. The 10kTrees website: A new online resource
289 for primate phylogeny. *Evol. Anthropol.* 19, 114–118.

290 Blomberg, S.P., Garland, T., Ives, A.R., 2003. Testing for phylogenetic signal in comparative
291 data: behavioral traits are more labile. *Evolution* 57, 717–745.

292 Bookstein, F.L., 2019. Pathologies of between-groups principal components analysis in
293 geometric morphometrics. *Evol. Biol.* 46, 271–302.

294 Cardini, A., Polly, P.D., 2020. Cross-validated between group PCA scatterplots: A solution to
295 spurious group separation? *Evol. Biol.* 47, 85–95.

296 Cardini, A., O'Higgins, P., Rohlf, F.J., 2019. Seeing distinct groups where there are none:
297 Spurious patterns from between-group PCA. *Evol. Biol.* 46, 303–316.

298 Collyer, M.L., Adams, D.C. 2018. RRPP: An R package for fitting linear models to high-
299 dimensional data using residual randomization. *Methods Ecol. Evol.* 9, 1772–1779.

300 Da Silva, A.R., 2020. On testing for seed sample heterogeneity with the exact probability
301 distribution of the germination count range. *Seed Sci. Res.* 30, 59-63.

302 Harrison, T., 1987. The phylogenetic relationships of the early catarrhine primates: A review
303 of the current evidence. *J. Hum. Evol.* 16, 41–80.

304 Harrison, T., 2010. Dendropithecoidea, Proconsuloidea, and Hominoidea (Catarrhini,
305 Primates). In: Werdelin, L., Sanders, W.J. (Eds.), *Cenozoic Mammals of Africa*. University
306 of California Press, Berkeley, pp. 429–469.

307 Ishida, H., Kunimatsu, Y., Nakatsukasa, M., Nakano, Y. 1999. New hominoid genus from the
308 Middle Miocene of Nachola, Kenya. *Anthropol. Sci.* 107. 189–191

309 Ishida, H., Kunimatsu, Y., Takano, T., Nakano, Y., Nakatsukasa, M., 2004. *Nacholapithecus*
310 skeleton from the Middle Miocene of Kenya. *J. Hum. Evol.* 46, 69–103.

311 Kikuchi, Y., Nakano, Y., Nakatsukasa, M., Kunimatsu, Y., Shimizu, D., Ogihara, N.,
312 Tsujikawa, H., Takano, T., Ishida, H., 2012. Functional morphology and anatomy of
313 cervical vertebrae in *Nacholapithecus kerioi*, a middle Miocene hominoid from Kenya. *J.*
314 *Hum. Evol.* 62, 677-695.

315 Kikuchi, Y., Nakatsukasa, M., Nakano, Y., Kunimatsu, Y., Shimizu, D., Ogihara, N.,
316 Tsujikawa, H., Takano, T., Ishida, H., 2015. Morphology of the thoracolumbar spine of the
317 middle Miocene hominoid *Nacholapithecus kerioi* from northern Kenya. *J. Hum. Evol.* 88,
318 25-42.

319 Kikuchi, Y., Nakatsukasa, M., Nakano, Y., Kunimatsu, Y., Shimizu, D., Ogihara, N.,

320 Tsujikawa, H., Takano, T., Ishida, H., 2016. Sacral vertebral remains of the Middle
321 Miocene hominoid *Nacholapithecus kerioi* from northern Kenya. *J. Hum. Evol.* 94, 117-
322 125.

323 Kunimatsu, Y., Nakatsukasa, M., Shimizu, D., Nakano, Y. and Ishida, H. 2019. Loss of the
324 subarcuate fossa and the phylogeny of *Nacholapithecus*. *J. Hum. Evol.* 131, 22–7.

325 Larson, S.G., 1998. Parallel evolution in the hominoid trunk and forelimb. *Evol. Anthropol.* 6,
326 87–99.

327 Le Gros Clark, W.E., Thomas, D.P., 1951. Associated jaws and limb bones of *Limnopithecus*
328 *macinnesi*. *Fossil Mammals Afr.* 3, 1–27.

329 McCrossin, L.M., Benefit, B.R., Giteu, S.N., Palmer, A.K., Blue, K.T., 1998. Fossil evidence
330 for the origins of terrestriality among Old World higher primates. In: Strasser, E., Fleagle,
331 J., Rosenberger, A., McHenry, H. (Eds.), *Primate Locomotion: Recent Advances*. Plenum
332 Press, New York, pp. 353–396.

333 McNulty, K.P., Begun, D.R., Kelley, J., Manthi, F.K., Mbua, E.N., 2015. A systematic
334 revision of *Proconsul* with the description of a new genus of early Miocene hominoid. *J.*
335 *Hum. Evol.* 84, 42–61.

336 Mitteroecker, P., Bookstein, F., 2011. Linear discrimination, ordination, and the visualization
337 of selection gradients in modern morphometrics. *Evol. Biol.* 38, 100–114.

338 Morimoto, N., Kunimatsu, Y., Nakatsukasa, M., Ponce de Leon, M.S., Zollikofer, C.P.,
339 Ishida, H., Sasaki, T. Suwa, G. 2020. Variation of bony labyrinthine morphology in Mio-
340 Plio–Pleistocene and modern anthropoids. *Am. J. Phys. Anthropol.* 173, 276–292.

341 Nakatsukasa, M., Kunimatsu, Y. 2009. *Nacholapithecus* and its importance for understanding
342 hominoid evolution. *Evol. Anthropol.* 18, 103–119.

343 Nakatsukasa, M., Yamanaka, A., Kunimatsu, Y., Shimizu, D., Ishida, H. 1998. A newly
344 discovered *Kenyapithecus* skeleton and its implications for the evolution of positional
345 behavior in Miocene East African hominoids. *J. Hum. Evol.* 34, 657–664.

346 Nakatsukasa, M., Kunimatsu, Y., Nakano, Y., Ishida, H. 2002. Morphology of hallucial
347 phalanges in extant anthropoids and fossil hominoids. *Z. Morphol. Anthropol.* 83, 361–
348 372.

349 Nakatsukasa, M., Kunimatsu, Y., Nakano, Y., Takano, T., Ishida, H. 2003a. Comparative and
350 functional anatomy of phalanges in *Nacholapithecus kerioi*, a Middle Miocene hominoid
351 from northern Kenya. *Primates* 44, 371–412.

352 Nakatsukasa, M., Tsujikawa, H., Shimizu, D., Takano, T., Kunimatsu, Y., Nakano, Y., Ishida
353 H. 2003b. Definitive evidence for tail loss in *Nacholapithecus*, and East African Miocene
354 hominoid. *J. Hum. Evol.* 45, 179–186.

355 Nakatsukasa, M., Kunimatsu, Y., Nakano, Y., Ishida, H. 2007a. Vertebral morphology of
356 *Nacholapithecus kerioi* based on KNM-BG 35250. *J. Hum. Evol.* 52, 347–369.

357 Nakatsukasa, M., Kunimatsu, Y., Nakano, Y., Egi, N., Ishida, H. 2007b. Postcranial bones of
358 infant *Nacholapithecus*: ontogeny and positional behavioral adaptation. *Anthropol. Sci.*
359 115, 201-213.

360 Nakatsukasa, M., Kunimatsu, Y., Shimizu, D., Nakano, Y., Kikuchi, Y., Ishida, H. 2012.
361 Hind limb of the *Nacholapithecus kerioi* holotype and implications for its positional
362 behavior. *Anthropol. Sci.* 120, 12073.

363 Nakatsukasa, M., Almécija, S., Begun, D.R. 2016. The hands of Miocene hominoids. In:
364 Kivell, T.L., Lemelin, P., Richmond, B.G., Schmitt, D. (Eds.), *The evolution of the primate*
365 *hand*. Springer, New York, pp. 485–514.

366 Kunimatsu, Y., Nakatsukasa, M., Shimizu, D., Nakano, Y., Ishida, H., 2019. Loss of the
367 subarcuate fossa and the phylogeny of *Nacholapithecus*. *J. Hum. Evol.* 131, 22–27.

368 Ogihara, N., Almécija, S., Nakatsukasa, M., Nakano, Y., Kikuchi, Y., Kunimatsu, Y.,
369 Makishima, H., Shimizu, D., Takano, T., Tsujikawa, H., Kagaya, M., Ishida, H. 2016.
370 Carpal bones of *Nacholapithecus kerioi*, a Middle Miocene hominoid from Northern
371 Kenya. *Am. J. Phys. Anthropol.* 160, 469–482.

372 Pagel, M., 1999. Inferring the historical patterns of biological evolution. *Nature* 401, 877–
373 884.

374 Patel, B.A., 2005. The hominoid proximal radius: Re-interpreting locomotor behaviors in
375 early hominins. *J. Hum. Evol.* 48, 415–432.

376 Pina, M., Kikuchi, Y., Nakatsukasa, M., Nakano, Y., Kunimatsu, Y., Ogiwara, N., Shimizu,
377 D., Takano, T., Tsujikawa, H., Ishida, H., 2021. New femoral remains of *Nacholapithecus*
378 *kerioi*: Implications for intraspecific variation and Miocene hominoid evolution. *J. Hum.*
379 *Evol.* 155, 102982.

380 Pugh, K.D. 2022. Phylogenetic analysis of Middle-Late Miocene apes. *J. Hum. Evol.* 165,
381 103140.

382 R Core Team, 2021. R: A language and environment for statistical computing. R Foundation
383 for Statistical Computing, Vienna.

384 Revell, L.J., 2012. Phytools: An R package for phylogenetic comparative biology (and other
385 things). *Methods Ecol. Evol.* 3, 217–223.

386 Rose, M.D., 1988. Another look at the anthropoid elbow. *J. Hum. Evol.* 17, 193–224.

387 Rose, M.D., 1993. Locomotor anatomy of Miocene hominoids. In: Gebo, D.L. (Ed.),
388 *Postcranial Adaptation in Nonhuman Primates*. Northern Illinois University Press,
389 DeKalb, pp. 252–272.

390 Rose, M.D., 1994. Quadrupedalism in some Miocene catarrhines. *J. Hum. Evol.* 26, 387–411.

391 Rose, M.D., 1997. Functional and phylogenetic features of the forelimb in Miocene
392 hominoids. In: Begun, D.R., Ward, C.V., Rose, M.D. (Eds.), *Function, Phylogeny and*
393 *Fossils: Miocene Hominoid Evolution and Adaptation*. Plenum Press, New York, pp. 79–
394 100.

395 Rose, M.D., Leakey, M.G., Leakey, R.E.F., Walker, A.C., 1992. Postcranial specimens of
396 *Simiolus enjiessi* and other primitive catarrhines from the early Miocene of Lake Turkana,
397 Kenya. *J. Hum. Evol.* 22, 171–237.

398 Rose, M.D., Nakano, Y., Ishida, H. 1996. *Kenyapithecus* postcranial specimens from
399 Nachola, Kenya. *Afr. Study Monogr.* 24, 3–56.

400 Rossie, J.B., Gutierrez, M., Goble, E., 2012. Fossil forelimbs of *Simiolus* from Moruorot,
401 Kenya. *Am. J. Phys. Anthropol.* 147 (S54), 252.

402 Ruff, C.B., 2002. Long bone articular and diaphyseal structure in Old World monkeys and
403 apes. I: Locomotor effects. *Am. J. Phys. Anthropol.* 119, 305–342.

404 Ruff, C.B., 2003. Long bone articular and diaphyseal structure in Old World monkeys and
405 apes. II: Estimation of body mass. *Am. J. Phys. Anthropol.* 120, 16–37.

406 Sawada, Y., Pickford, M., Itaya, T., Makinouchi, T., Tateishi, M., Kabeto, K., Ishida, S.,
407 Ishida, H., 1998. K-Ar ages of Miocene Hominoidea (*Kenyapithecus* and
408 *Samburupithecus*) from Samburu Hills, Northern Kenya. *C. R. Acad. Sci. Paris* 326, 445–
409 451.

410 Sawada, Y., Saneyoshi, M., Nakayama, K., Sakai, T., Itaya, T., Hyodo, M., Mukokya, Y.,
411 Pickford, M., Senut, B., Tanaka, S., Chujo, T., Ishida, H. 2006. The ages and geological
412 background of Miocene hominoids *Nacholapithecus*, *Samburupithecus*, and *Orrorin* from
413 Kenya. In: H. Ishida, R. Tuttle, M. Pickford, N. Ogihara, M. Nakatsukasa (Eds.), *Human*
414 *origins and environmental backgrounds. Developments in Primatology: Progress and*
415 *Prospects.* Springer, New York, pp. 71-96

416 Schlager, S., 2017. Morpho and Rvcg – shape analysis in R: R-packages for geometric
417 morphometrics, shape analysis and surface manipulations. In: Zheng, G., Li, S., Székely,
418 G. (Eds.), *Statistical Shape and Deformation Analysis. Methods, Implementation and*
419 *Applications.* Academic Press, London, pp. 217–256.

420 Senut, B., 1989. *Le Coude des Primates Hominoïdes. Anatomie, Fonction, Taxonomie,*
421 *Évolution.* Éditions du Centre National de la Recherche Scientifique, Paris.

422 Senut, B., Nakatsukasa, M., Kunimatsu, Y., Nakano, Y., Takano, T., Tsujikawa, H., Shimizu,
423 D., Kagaya, M., Ishida, H. 2004. Preliminary analysis of *Nacholapithecus* scapula and
424 clavicle from Nachola, Kenya. *Primates* 45, 97-104.

425 Sherwood, R.J., Ward, R.J., Hill, A., Duren, D.L., Brown, B., Downs, W., 2002. Preliminary
426 description of the *Equatorius africanus* partial skeleton KNM-TH 28860 from
427 Kipsaramon, Tugen Hills, Baringo District, Kenya. *J. Hum. Evol.* 42, 63–73.

428 Takano, T., Nakatsukasa, M., Kunimatsu, Y., Nakano, N., Ogihara N., Ishida, H. 2018.
429 Forelimb long bones of *Nacholapithecus* (KNM-BG 35250) from the middle Miocene in
430 Nachola, northern Kenya. *Anthropol. Sci.* 126, 135–149.

431 Takano, T., Nakatsukasa, M., Pina, M., Kunimatsu, Y., Nakano, Y., Morimoto, N., Ogihara,
432 N., Ishida, H. 2020. New forelimb long bone specimens of *Nacholapithecus kerioi* from
433 the Middle Miocene of northern Kenya. *Anthropol. Sci.* 128, 200116.

434 Urciuoli, A., Zanolli, C., Almecija, S., Alba, D.M. 2020. Reassessment of the phylogenetic
435 relationships of the late Miocene apes *Hispanopithecus* and *Rudapithecus* based on
436 vertibular morphology. *Proc. Natl. Acad. Sci. USA* 118, e2015215118.

437 Walker, A.C., Pickford, M., 1983. New postcranial fossils of *Proconsul africanus* and
438 *Proconsul nyanzae*. In: Ciochon, R.L., Corruccini, R.S. (Eds.), *New Interpretations of Ape*
439 *and Human Ancestry*. Plenum Press, New York, pp. 325–351.

440 Ward, C.V., 1993. Torso morphology and locomotion in *Proconsul nyanzae*. *Am. J. Phys.*
441 *Anthropol.* 92, 291–328.

442 Ward, C.V., 2015. Postcranial and locomotor adaptations of hominoids. In: Henke, W.,
443 Tattersall, I. (Eds.), *Handbook of Paleoanthropology*, 2nd ed. Springer, Heidelberg, pp.
444 1363–1386.

445 Ward, C.V., Walker, A., Teaford, M.F., Odhiambo, L., 1993. Partial skeleton of *Proconsul*
446 *nyanzae* from Mfangano Island, Kenya. *Am. J. Phys. Anthropol.* 90, 77–111.

447 Ward, S., Brown, B., Hill, A., Kelley, J., Downs, W., 1999. *Equatorius*: A new hominoid

448 genus from the middle Miocene of Kenya. *Science* 285, 1382–1386.
449 Wiley, D.F., Amenta, N., Alcantara, D.A., Ghosh, D., Kil, Y.J., Delson, E., Harcourt-Smith,
450 W., Rohlf, F.J., St John, K., Hamann, B., 2005. Evolutionary morphing. In: Silva, T.C.,
451 Gorller, E., Rushmeier, H. (Eds.), VIS 05 IEEE Visualization. IEEE, Minneapolis, pp.
452 431–438.
453 Zapfe, H., 1958. The skeleton of *Pliopithecus (Epipliopithecus) vindobonensis* Zapfe and
454 Hürzeler. *Am. J. Phys. Anthropol.* 16, 441–457.
455 Zapfe, H., 1961. Die Primatenfunde aus der miozänen Spaltenfüllung von Neudorf an der
456 March (Děvínská Nová Ves), Tschechoslowakei. *Schweizer. Palaeontol. Abh.* 78, 1–293.

457

458 **Figure captions**

459

460 **Figure 1.** Right proximal radial fragment (KNM BG 40021) of *Nacholapithecus kerioi* from
461 the Aka Aiteputh Formation in Nachola, Kenya, in proximal (a), anterior (b), and medial (c)
462 views.

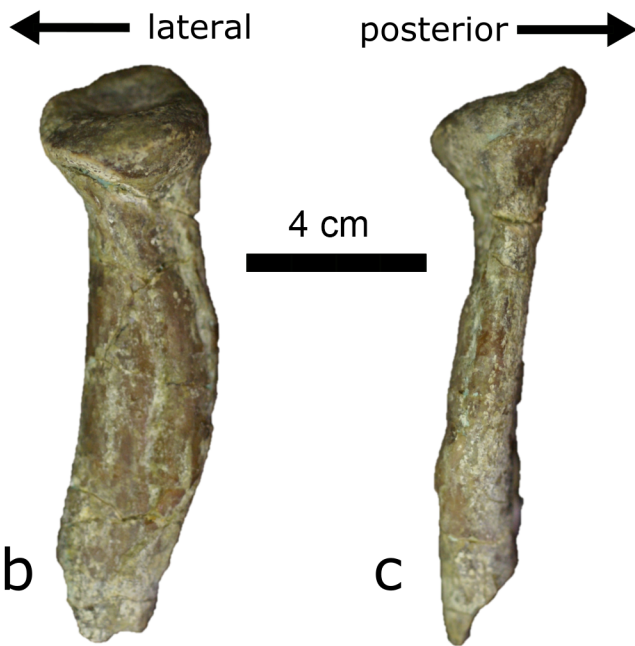
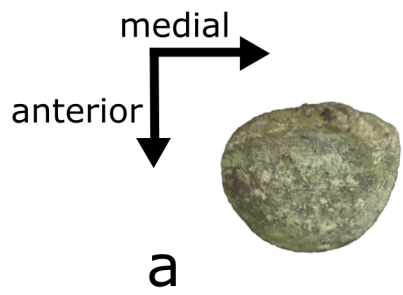
463

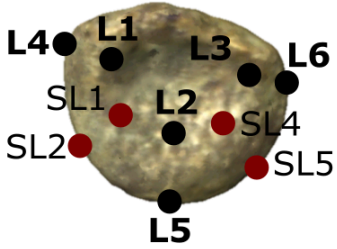
464 **Figure 2.** Landmark protocol illustrated on renderings of a 3D model of the right proximal
465 radial fragment (KNM-BG 40021, mirrored) of *Nacholapithecus kerioi*, in proximal (a),
466 anterior (b), lateral (c), and medial (d) views. Landmarks (L, bolded) and semilandmarks (SL)
467 are denoted by black and red dots, respectively, and described in SOM Table S3.

468

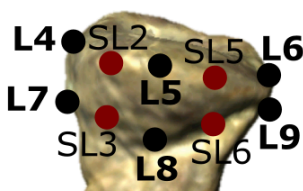
469 **Figure 3.** Results of the between-group principal component analysis as depicted by a
470 bivariate plot of bgPC2 vs. bgPC1. Groups distinguished a priori are denoted by color coded
471 convex hulls and symbols: violet = hominids; green = hylobatids; orange = cercopithecines;
472 emerald = colobines; pink = platyrrhines. Extant genera are denoted by different symbols (see
473 legend). The scatter of *Ateles* is highlighted with a convex hull in darker pink within the

474 platyrrhine distribution. Fossil specimens (scores projected a posteriori) are denoted by
475 colored stars (see legend). The percentage of variance explained by each bgPC is reported
476 within parentheses. Renderings along axes represent maximum and minimum shape changes
477 for that axis (corresponding to their position at the positive and negative ends of each axis).
478 Abbreviation: bgPC = between-group principal component.

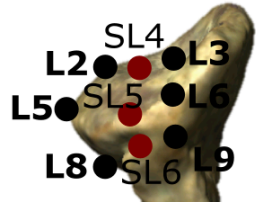




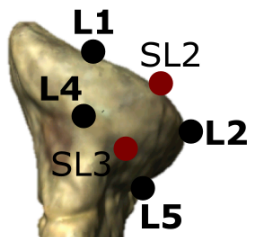
a



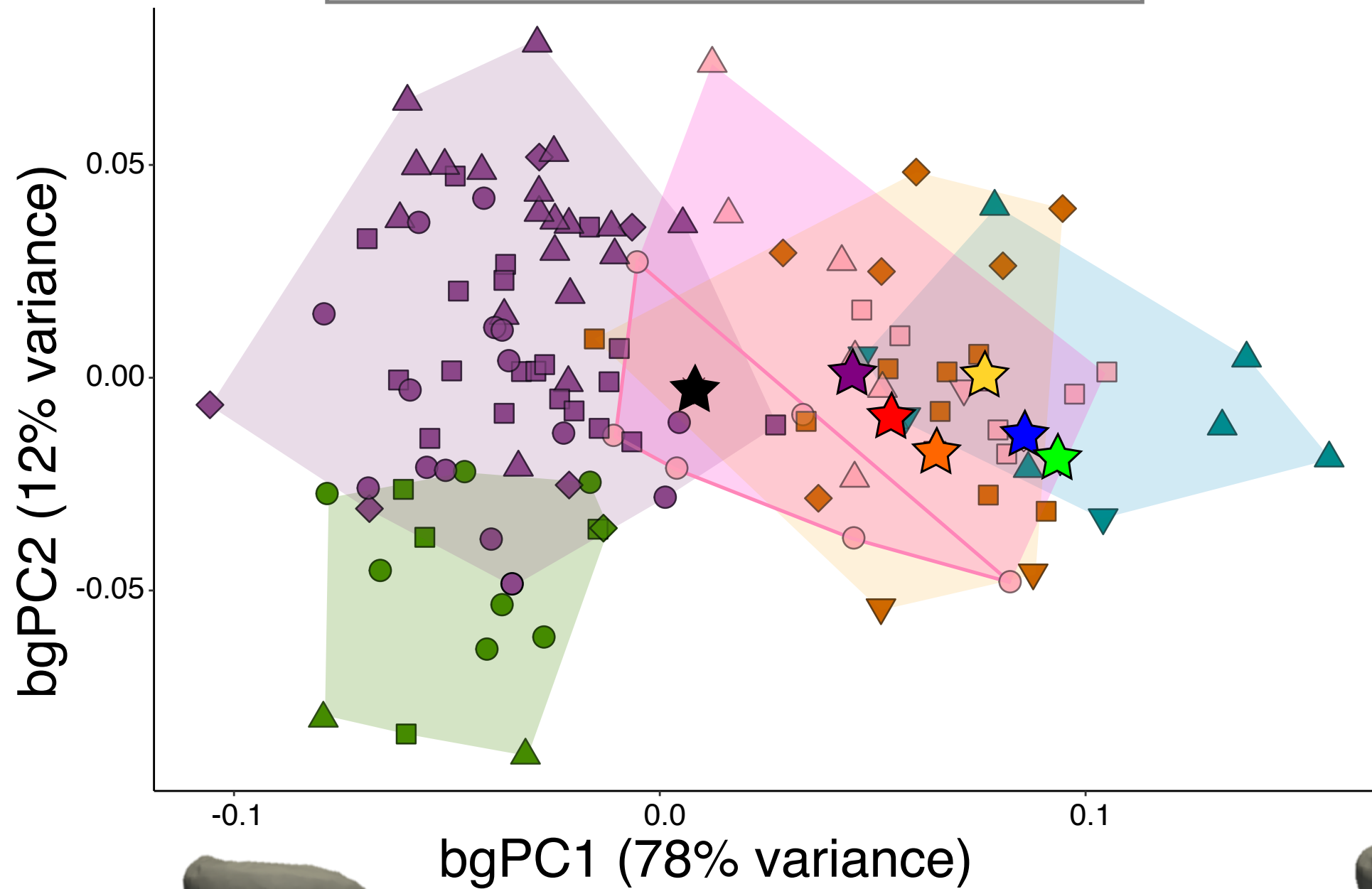
b



c



d



- ★ *Ekembo heseloni* (KNM-RU 2036AI)
- ★ *Simiolus enjessi* (KNM-MO 63)
- ★ *Simiolus enjessi* (KNM-MO 17022B)
- ★ *Epipliopithecus vindobonensis* (OE 304PCe)
- ★ *Dendropithecus macinnesi* (KNM-RU 2098)
- ★ *Equatorius africanus* (KNM-TH 28860J)
- ★ *Nacholapithecus kerioi* (KNM-BG 40021)

- *Gorilla*
- ▲ *Pongo*
- *Pan*
- ◆ *Homo*
- ◆ *Nomascus*
- *Hylobates*
- *Symphalangus*
- ▲ *Hoolock*
- ▼ *Mandrillus*
- *Macaca*
- ◆ *Papio*
- ▼ *Colobus*
- ▲ *Nasalis*
- ▲ *Alouatta*
- *Cebus*
- *Ateles*
- ▼ *Lagothrix*

Table 1

Squared Mahalanobis distances (D^2) between fossils and group means, and classification results based on typicality probabilities (p) of the fossils computed from the between-group principal component analysis of radial head shape.^a

Species	Catalogue No.	D^2/p	Cercopithecines	Colobines	Hominids	Hylobatids	Platyrrhines
<i>Nacholapithecus kerioi</i>	KNM-BG 40021	D^2	9.892	8.325	7.317	6.062	1.782
		p	0.014	0.010	0.217*	0.015	0.486**
<i>Ekembo heseloni</i>	KNM-RU 2036CE	D^2	3.878	5.265	4.770	11.891	0.603
		p	0.529*	0.107	0.062	0.002	0.983**
<i>Equatorius africanus</i>	KNM-TH 28860-J	D^2	4.002	4.385	11.520	7.729	2.919
		p	0.689*	0.155	0.007	0.001	0.827**
<i>Epipliopithecus vindobonensis</i>	O.E. 304 PCe	D^2	7.576	17.238	10.630	16.416	5.385
		p	0.127**	<0.001	<0.001	<0.001	0.056*
<i>Dendropithecus macinnesi</i>	KNM-RU 2098	D^2	15.063	8.5177	12.022	13.748	1.964
		p	0.031	0.118*	0.004	<0.001	0.874**
<i>Simiolus enjiessi</i>	KNM-MO 63	D^2	12.904	12.547	13.622	14.547	3.052
		p	0.528**	0.011	<0.001	<0.001	0.233*

<i>Simiolus enjiessi</i>	KNM-MO 17022B	D ²	5.533	11.160	16.496	11.045	6.580
		<i>p</i>	0.304**	0.003	<0.001	<0.001	0.088*

^a Group membership was rejected at $p < 0.05$. Two asterisks (**) denote primary group classification; one asterisk (*) denotes secondary group classification. Shortest D² and highest *p*-values are bolded.

Supplementary Online Material (SOM):

The radial head of the Middle Miocene ape *Nacholapithecus kerioi*: Morphometric affinities, locomotor inferences, and implications for the evolution of the hominoid humeroradial joint

SOM S1

Supplementary materials and methods

Scanning

The radii of *Simiolus enjiessi* KNM-RU 17022B and of *Epipliopithecus vindobonensis* O.E. 304 PCE were scanned from high-quality casts housed in the Institut Català de Paleontologia Miquel Crusafont (ICP, Cerdanyola del Vallès, Spain). All the other fossils (see SOM Table S1) were scanned from original specimens at the Kenya National Museums with a NextEngine surface laser scanner (Next Engine, Santa Monica) using the HD3 macro mode. The 3D models of the extant specimens were obtained using a NextEngine surface scanner and two different high-resolution μ CT scanners (SOM Table S2): a BIR ACTIS 225/300 industrial μ CT scanner (Department of Human Evolution, Max Planck Institute for Evolutionary Anthropology, Germany) and a Nikon XT 225 ST μ CT scanner (Cambridge Biotomography Centre, Department of Zoology, University of Cambridge, UK). Specimens scanned with the NextEngine scanner were obtained using a resolution of $>10,000$ points per square inch; 6–12 scans were taken at two or more positions and then merged using ScanStudio HD PRO software v. 1.3.2 (Next Engine, Santa Monica). The isotropic voxel size range for the μ CT scans sample is 21.9–51.5 μ m. Laser scan-derived 3D models were cleaned (fill holes, irregularities in mesh, etc.) using Geomagic Wrap 2017 (3D Systems, Inc. Morrisville), and μ CT scans were processed in AVIZO v. 6.3 (Visualization Sciences Group, Berlin).

Landmark protocol

Our landmark protocol was specifically devised to capture the shape affinities of KNM-BG 40021. It consists of 15 3D landmarks including 9 type II and 6 semilandmarks (Fig. 2; SOM Table S3). Type II landmarks reflect points in anatomical structures that can be recognized by their geometry, such as the maximum point of a curve. The homology of type III landmarks is given relative to the other landmarks around them, which should be type I or type II (therefore, a type III landmark would be the middle point between two 'true' landmarks, for example; Bookstein, 1997; O'Higgins, 2000). The protocol thus captures the anterior aspect of the radial head, including the anterior outline of the fovea (L1–3, SL1–2), the anterior outline of the radial head (L4–6, SL3–4), and the distal expansion of articular surface (L7–9, SL5–6). Radii were oriented in anterior view, either using anatomical orientation (complete radii) or based on the anteromedial position of the radial tuberosity, which was preserved in all individuals, allowing a swift identification of the medial, lateral, and posterior aspects of the radial head (as type II landmarks depend on correct orientation for placement; Zelditch et al., 2012). All type II

landmarks (L1–9) were used in a previous study of the proximal radius of fossil catarrhines (Arias-Martorell et al., 2021). We included six additional semilandmarks to ensure a more detailed and accurate representation of the anterior aspect of the shape of the radial head (Bookstein, 1997). Shape changes occurring along the axes of the bgPCA depicted in Figure 3 were visualized by warping the specimen closest to the mean configuration—identified with the ‘findMeanSpec’ function in Geomorph (Adams et al., 2020)—toward the extreme landmark configurations for each bgPC.

Statistics

We computed the standard deviates of observed statistics as effect sizes from distributions of random outcomes. We used these to compare the strength of morphological integration across morphometric datasets using the statistic test (Z-score) under the null hypothesis of a random association of variables. The method displays a constant expected value and confidence intervals and thus provides a consistent measure of integration suitable for comparisons across datasets (Adams and Collyer, 2016).

To assess the similarity of a fossil specimen’s score to each a priori defined group based on their distribution of scores (variability) we used typicality probabilities. These are computed based on the Mahalanobis square distance (D^2) between the specimen and the group centroids and represent the p -value to test the null hypothesis of group membership. Hence, a specimen is considered an outlier for a given group when $p < 0.05$, while higher typicality probabilities denote closer affinities between the individual and the distribution of the group. Note that the sum of the typicality probabilities for a given specimen does not equal 1, as they do not assume that the specimen must belong to one of the groups defined a priori, and rather represent the likelihood of belonging to each a priori defined group separately. In the UPGMA analysis, we used the mean Procrustes coordinates of each group, of the two *Simiolus* specimens, and the other fossils.

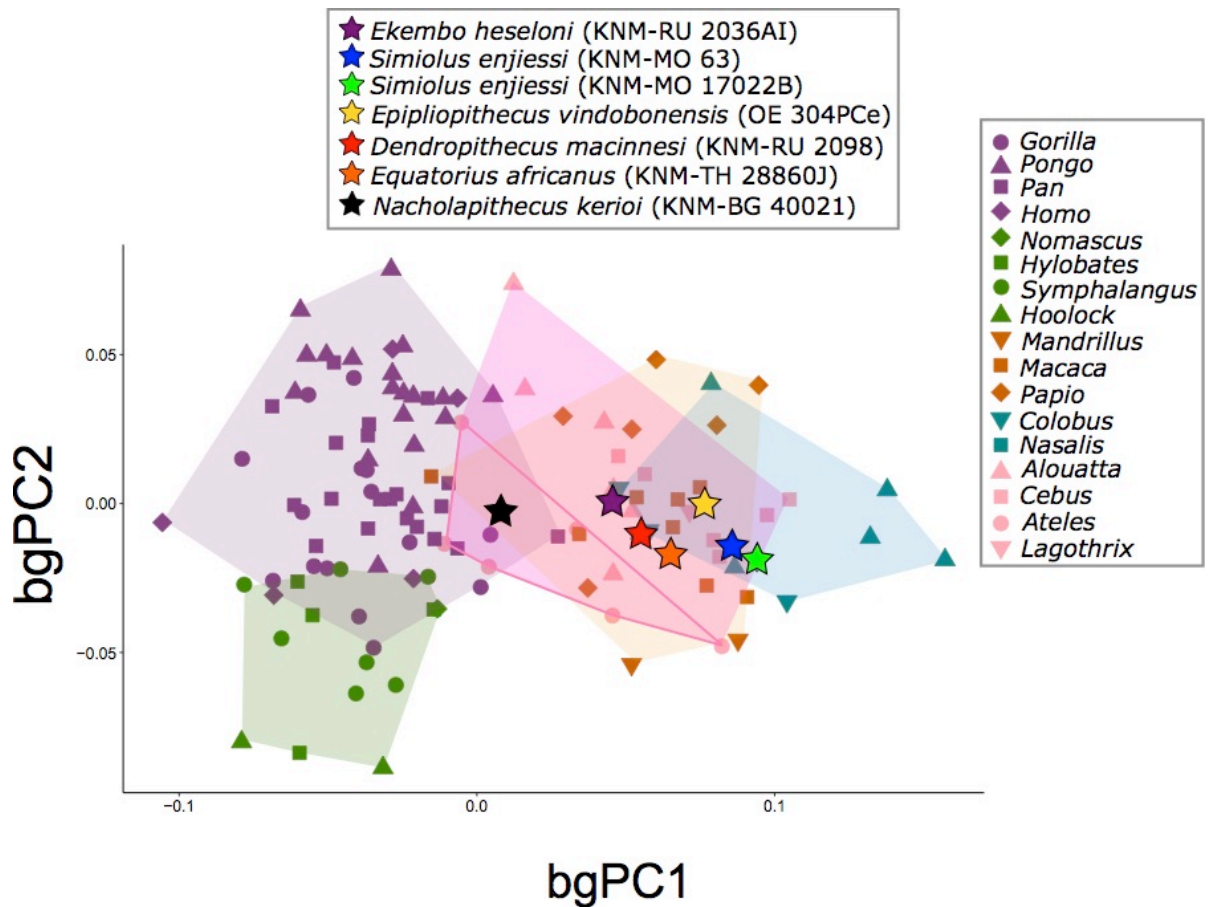
To compute the amount of phylogenetic signal embedded in the shape data we computed both Pagel’s λ (Pagel, 1999; Freckleton et al., 2002) and Bloomberg’s K (Blomberg et al., 2003) statistics. Both compare the observed data distribution to that expected under a Brownian motion model of evolution but they are not entirely comparable: λ compares the actual covariance among species with that expected under Brownian motion, whereas K more specifically reflects how variance is partitioned. Pagel’s λ ranges from 0 to 1: $\lambda = 1$ implies that trait covariance is exclusively influenced by phylogeny, $\lambda < 1$ suggests that other factors besides phylogeny influence trait evolution, and $\lambda = 0$ is obtained when no phylogenetic

correlation is found in the data. In contrast, Blomberg's K may vary beyond unity: $K \approx 1$ similarly implies a model of evolution that closely resembles that expected under Brownian motion, $K < 1$ implies that closely related taxa resemble each other less than expected (variance accumulates within clades), possibly because of independent evolution (i.e., homoplasy), and $K > 1$ implies that closely related taxa are more similar than expected, so that variance accumulates among clades (as the result of stabilizing selection or architectural constraints).

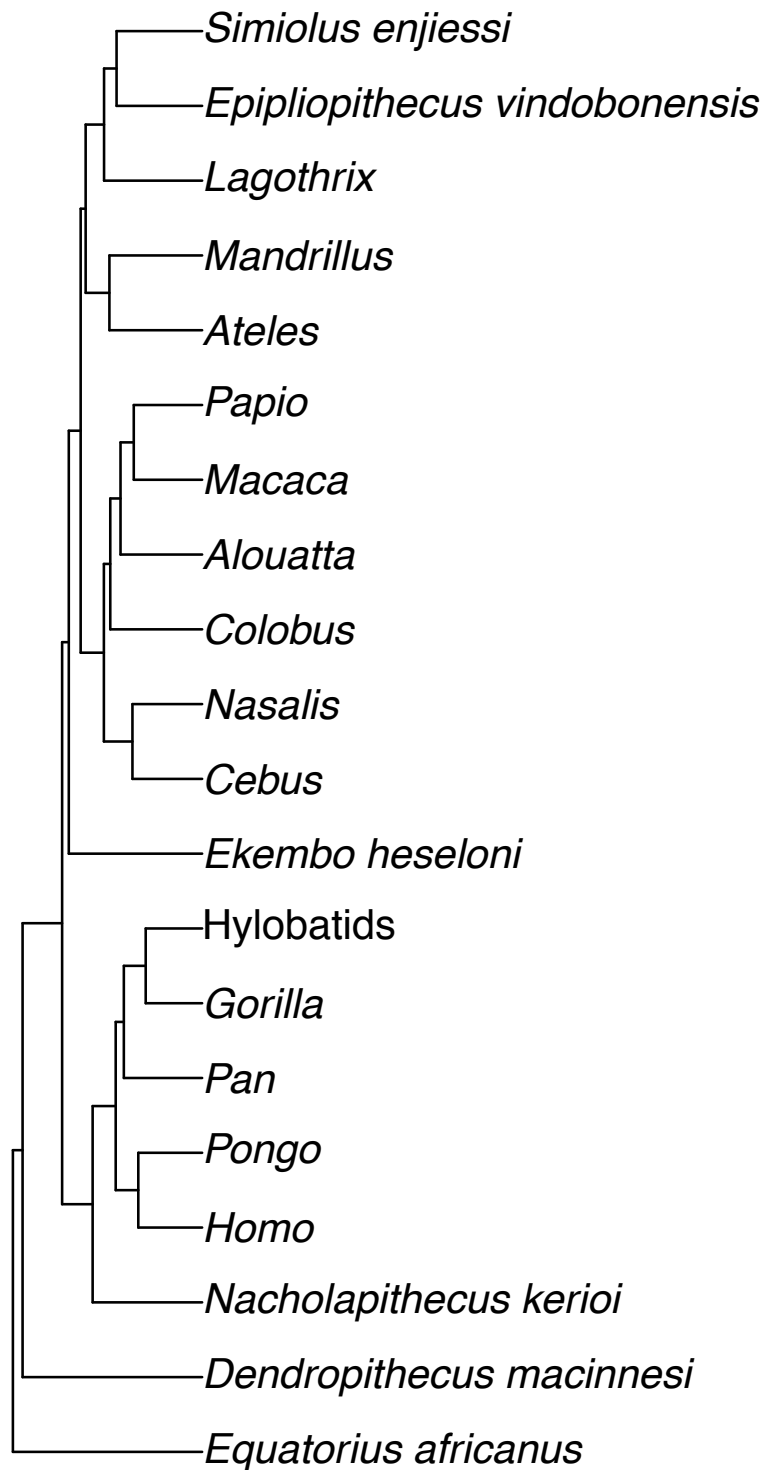
SOM S2

Supplementary results

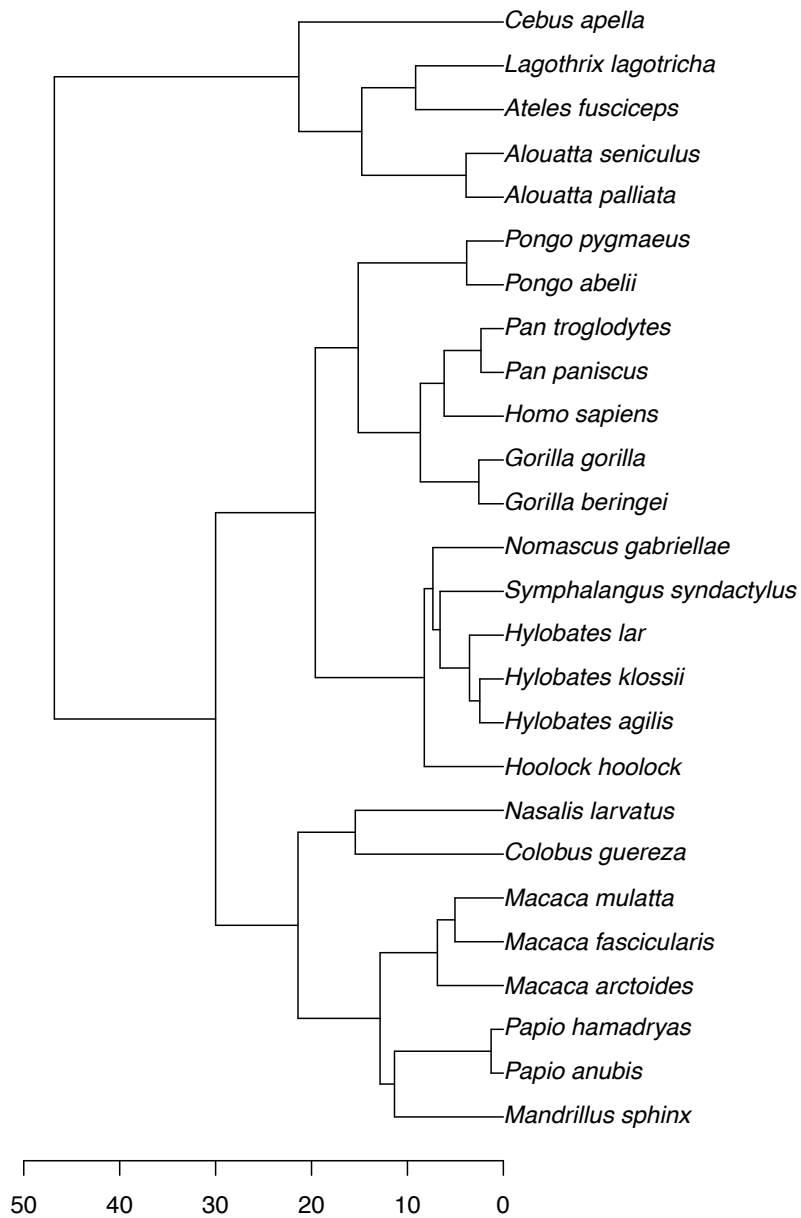
Shape changes were warped onto the specimen of *Pan troglodytes* USNM-220062, which was identified to be the closest to the mean configuration with a Mahalanobis distance of 0.068. In the UPGMA analysis, all the monkeys clustered together, including a subcluster for *Lagothrix*, *Simiulus*, and *Epipliopithecus*, apart from the hominoid + *Nacholapithecus* cluster. *Ekembo* did not cluster with any other taxon but is at the base of the monkey + small fossil catarrhines cluster, whereas *Equatorius* and *Dendropithecus* clustered apart from all the other taxa.



SOM Figure S1. Results of the cross-validated between-group principal component (bgPC) analysis of proximal radial shape among extant anthropoid primates as depicted by a bivariate plot of bgPC2 vs. bgPC1. Groups distinguished a priori are denoted by color-coded convex hulls and symbols: violet = hominids; green = hylobatids; orange = cercopithecines; emerald = colobines; pink = platyrrhines. The scatter of *Ateles* is highlighted with a convex hull in darker pink within the platyrrhine distribution. Extant genera are denoted by different symbols (see legend). Fossil specimens (scores projected a posteriori) are denoted by colored stars (see legend).



SOM Figure S2. Dendrogram derived from the unweighted pair group methods with arithmetic mean (UPGMA) cluster analysis. Cophenetic correlation was $r^2 = 0.84$.



SOM Figure S3. Consensus molecular tree downloaded from 10kTrees website v. 3 (www.10Ktrees.org) used to compute phylogenetic signal and conduct the phylogenetic generalized least squares analyses.

SOM Table S1

Details of the fossil comparative sample.

Species	Catalogue no.	Site	References
<i>Simiolus enjiessi</i>	KNM-MO 63	Moruorot	Rose et al. (1992: Fig. 8); Senut (1989: Fig. 62); Rossie et al. (2012)
<i>Simiolus enjiessi</i>	KNM-MO 17022B	Kalodirr	Rose et al. (1992: Fig. 9)
<i>Dendropithecus macinnesi</i>	KNM-RU 2098	Rusinga Island	Le Gros Clark and Thomas (1951: Pl. 4 Fig. 9, Pl. 5 Fig. 11); Senut (1989: Fig. 76 and Pl. X)
<i>Epipliopithecus vindobonensis</i>	O.E. 304 PCe	Devínska Nová Ves	Zapfe (1958: Pl. 1A and Fig. B5); Zapfe (1961: Fig. 54); Senut (1989: Fig. 95 and Pl. XV)
<i>Ekembo heseloni</i>	KNM-RU 2036CE	Rusinga Island	Walker and Pickford (1983: Fig. 4); Senut, 1989 (Fig. 74 and Pl. VII)
<i>Equatorius africanus</i>	KNM-TH 28860-J	Kipsaraman	Ward et al. (1999: Fig 2k); Sherwood et al. (2002: Fig. 1f)

SOM Table S2

Details of the extant primate sample used in the study. Media and identifier (when available) are listed for specimens downloaded from Morphosource.org.

Species	Catalog no.	Sex	Side	Source	Media	Identifier	Scanner
<i>Alouatta palliata aequatorialis</i>	USNM 338107	M	L	USNM	—	—	NextEngine
<i>Alouatta palliata palliata</i>	USNM 282798	F	L	USNM	—	—	NextEngine
<i>Alouatta seniculus</i>	AMNH 42316	F	L	AMNH	—	—	NextEngine
<i>Alouatta seniculus</i>	AMNH 23333	M	L	AMNH	—	—	NextEngine
<i>Alouatta</i> sp.	ZMB 35764	M	L	ZMB	—	—	μCT (BIR ACTIS)
<i>Alouatta</i> sp.	ZMS 1973-0330	?	R	ZMS	—	—	μCT (BIR ACTIS)
<i>Ateles fusciceps robustus</i>	USNM 338111	F	L	USNM	—	—	NextEngine
<i>Ateles fusciceps robustus</i>	USNM 338112	M	L	USNM	—	—	NextEngine
<i>Ateles</i> sp.	ZMB 45255	F	R	ZMB	—	—	μCT (BIR ACTIS)
<i>Ateles</i> sp.	ZMB 44814	M	R	ZMB	—	—	μCT (BIR ACTIS)
<i>Ateles</i> sp.	ZMB 38734	?	R	ZMB	—	—	μCT (BIR ACTIS)
<i>Ateles</i> sp.	ZMB 44079	?	L	ZMB	—	—	μCT (BIR ACTIS)
<i>Cebus apella apella</i>	USNM 361020	M	L	USNM	—	—	NextEngine
<i>Cebus apella</i>	USNM 397940	F	R	USNM	—	—	NextEngine
<i>Cebus apella</i>	AMNH 133606	M	L	AMNH	—	—	NextEngine
<i>Cebus apella paraguayanus</i>	AMNH 133631	M	R	MS	M12099-19605	urn:catalog:AMNH:Mammals:M-133631	—
<i>Cebus apella paraguayanus</i>	AMNH 133623	M	R	MS	M12095-19594	urn:catalog:AMNH:Mammals:M-133623	—
<i>Cebus apella paraguayanus</i>	AMNH 133628	M	R	MS	M12093-19588	urn:catalog:AMNH:Mammals:M-133628	—

<i>Colobus guereza</i>	AMNH 52223	F	L	AMNH	—	—	NextEngine
<i>Colobus guereza</i>	AMNH 52241	F	L	AMNH	—	—	NextEngine
<i>Colobus guereza kikuyuensis</i>	USNM 452621	M	L	USNM	—	—	NextEngine
<i>Colobus guereza</i>	AMNH 52248	M	L	AMNH	—	—	NextEngine
<i>Colobus guereza</i>	USNM 452632	F	L	USNM	—	—	NextEngine
<i>Gorilla beringei beringei</i>	AMNH 54091	F	L	AMNH	—	—	NextEngine
<i>Gorilla beringei beringei</i>	RMCA 2263	F	L	RMCA	—	—	NextEngine
<i>Gorilla beringei beringei</i>	USNM 395636	M	L	USNM	—	—	NextEngine
<i>Gorilla beringei beringei</i>	USNM 396934	M	L	Morphosource	M56720-102006	http://n2t.net/ark:/65665/313444cf4-f1e7-4bbc-ba69-039e4d4557e4	—
<i>Gorilla beringei beringei</i>	USNM 396937	F	L	Morphosource	M57009-102295	http://n2t.net/ark:/65665/32f41b8f5-9a15-4f88-af7e-8218ebf0b616	—
<i>Gorilla beringei beringei</i>	USNM 397351	M	L	Morphosource	M56268-101554	http://n2t.net/ark:/65665/3db306794-3c8e-4930-bb20-e514ac62bac6	—
<i>Gorilla beringei graueri</i>	AMNH 202932	M	R	AMNH	—	—	NextEngine
<i>Gorilla beringei graueri</i>	RMCA 8187	M	L	RMCA	—	—	NextEngine
<i>Gorilla beringei</i>	USNM 239883	M	L	USNM	—	—	NextEngine
<i>Gorilla gorilla</i>	USNM 586541	F	R	USNM	—	—	NextEngine
<i>Gorilla gorilla gorilla</i>	AMNH 1673390	F	L	AMNH	—	—	NextEngine
<i>Gorilla gorilla</i>	CMNH 2767	M	L	CMNH	—	—	NextEngine
<i>Gorilla gorilla</i>	USNM 174722	M	R	USNM	—	—	NextEngine
<i>Gorilla gorilla</i>	USNM 176225	M	L	USNM	—	—	NextEngine
<i>Gorilla gorilla</i>	MER 300	F	R	PCM	—	—	μCT (Nikon)
<i>Homo sapiens</i>	AMNH 99-8376	F	L	AMNH	—	—	NextEngine
<i>Homo sapiens</i>	USNM 1512	F	L	USNM	—	—	NextEngine
<i>Homo sapiens</i>	AMNH 20-3501	M	L	AMNH	—	—	NextEngine

<i>Homo sapiens</i>	USNM 942	M	L	USNM	—	—	NextEngine
<i>Homo sapiens</i>	PSU 105-1793	?	L	MS	M45359-82651	—	—
<i>Hoolock hoolock</i>	AMNH 83425	F	R	AMNH	—	—	NextEngine
<i>Hoolock hoolock</i>	AMNH 83420	M	R	AMNH	—	—	NextEngine
<i>Hylobates agilis</i>	AMNH 106575	F	L	AMNH	—	—	NextEngine
<i>Hylobates klossii</i>	AMNH 103344	M	R	AMNH	—	—	NextEngine
<i>Hylobates klossii</i>	AMNH 103347	M	L	AMNH	—	—	NextEngine
<i>Hylobates lar vestitus</i>	NMNH 271047	F	L	USNM	—	—	NextEngine
<i>Lagothrix lagothricha</i>	DU-BAA 90	?	R	MS	M12471-20497	ark:/87602/m4/M20497	—
<i>Macaca arctoides</i>	AMNH 112727	F	L	AMNH	—	—	NextEngine
<i>Macaca fascicularis</i>	USNM 271168	M	R	USNM	—	—	NextEngine
<i>Macaca fascicularis</i>	ZMB 48496	?	L	ZMB	—	—	μCT (BIR ACTIS)
<i>Macaca fascicularis</i>	ZMB 49090	?	L	ZMB	—	—	μCT (BIR ACTIS)
<i>Macaca fascicularis</i>	ZMB 49092	?	L	ZMB	—	—	μCT (BIR ACTIS)
<i>Macaca mulatta</i>	DU-BAA 142	?	R	MS	M12472-20500	—	—
<i>Macaca mulatta</i>	USNM 537241	F	L	USNM	—	—	NextEngine
<i>Macaca mulatta</i>	USNM 537253	M	L	USNM	—	—	NextEngine
<i>Mandrillus sphinx</i>	AMNH 89361	M	R	MS	M10169-14599	urn:catalog:AMNH:Mammals:M-89361	—
<i>Mandrillus sphinx</i>	AMNH 89365	M	R	MS	M10176-14633	urn:catalog:AMNH:Mammals:M-89365	—
<i>Nasalis larvatus</i>	USNM 536050	F	L	USNM	—	—	NextEngine
<i>Nasalis larvatus</i>	AMNH 106275	M	L	AMNH	—	—	NextEngine
<i>Nasalis larvatus</i>	AMNH 198276	M	L	USNM	—	—	NextEngine
<i>Nomascus gabriellae</i>	AMNH 87253	F	L	AMNH	—	—	NextEngine

<i>Pan paniscus</i>	AMNH 86857	F	L	AMNH	—	—	NextEngine
<i>Pan paniscus</i>	RMCA 29045	F	L	RMCA	—	—	NextEngine
<i>Pan paniscus</i>	RMCA 27696	M	R	RMCA	—	—	NextEngine
<i>Pan paniscus</i>	SBU 87-1	M	L	SBU	—	—	NextEngine
<i>Pan troglodytes</i>	USNM 176226	F	L	USNM	—	—	NextEngine
<i>Pan troglodytes</i>	USNM 176229	F	L	USNM	—	—	NextEngine
<i>Pan troglodytes</i>	USNM 176227	M	L	USNM	—	—	NextEngine
<i>Pan troglodytes</i>	USNM 220327	M	L	USNM	—	—	NextEngine
<i>Pan troglodytes</i>	USNM 395820	M	L	USNM	—	—	NextEngine
<i>Pan troglodytes</i>	USNM 481804	M	R	USNM	—	—	NextEngine
<i>Pan troglodytes schweinfurthii</i>	AMNH 51376	M	R	MS	M10175-14630	urn:catalog:AMNH:Mammals:M-51376	—
<i>Pan troglodytes schweinfurthii</i>	AMNH 51393	M	R	MS	M10242-14814	urn:catalog:AMNH:Mammals:M-51393	—
<i>Pan troglodytes troglodytes</i>	AMNH 54330	M	L	MS	M10240-14808	urn:catalog:AMNH:Mammals:M-54330	—
<i>Pan troglodytes troglodytes</i>	USNM 220064	F	L	USNM	—	—	NextEngine
<i>Pan troglodytes troglodytes</i>	USNM 220062	F	L	MS	M56889-102175	http://n2t.net/ark:/65665/3dcfb7753-f4d7-4334-9b52-6f9f1b9ea03e	—
<i>Pan troglodytes troglodytes</i>	USNM 220063	F	L	MS	M56483-101769	http://n2t.net/ark:/65665/386ed1f25-2f34-459d-91e5-d0111c2e0dc6	—
<i>Pan troglodytes verus</i>	MPI-EVA 11778	F	L	MPI	—	—	μCT (BIR ACTIS)
<i>Pan troglodytes verus</i>	MPI-EVA 13429	F	L	MPI	—	—	μCT (BIR ACTIS)
<i>Pan troglodytes verus</i>	MPI-EVA 15001	F	L	MPI	—	—	μCT (BIR ACTIS)
<i>Pan troglodytes verus</i>	AMNH 89406	M	L	AMNH	—	—	NextEngine
<i>Papio anubis</i>	AMNH 52668	F	L	AMNH	—	—	NextEngine

<i>Papio anubis</i>	AMNH 120388	M	L	AMNH	—	—	NextEngine
<i>Papio anubis neumanni</i>	USNM 384235	F	L	USNM	—	—	NextEngine
<i>Papio anubis neumanni</i>	USNM 384229	M	L	USNM	—	—	NextEngine
<i>Papio hamadryas</i>	ZMB 105450	M	R	ZMB	—	—	μCT (BIR ACTIS)
<i>Papio hamadryas</i>	ZMB 65265	M	L	ZMB	—	—	μCT (BIR ACTIS)
<i>Pongo abelii</i>	USNM 588109	F	L	USNM	—	—	NextEngine
<i>Pongo abelii</i>	USNM 143588	M	L	USNM	—	—	NextEngine
<i>Pongo abelii</i>	USNM 143587	M	L	MS	M56592-101878	http://n2t.net/ark:/65665/33bd6f2f4-8b1a-4ffd-966f-06506fd24428	—
<i>Pongo abelii</i>	USNM 143590	M	L	MS	M56324-101610	http://n2t.net/ark:/65665/389dc210f-f5b3-4910-ae87-a26700227801	—
<i>Pongo abelii</i>	USNM 143593	M	L	MS	M56494-101780	http://n2t.net/ark:/65665/329ae2628-4c93-4da7-8e52-5f0c1e7bcc9e	—
<i>Pongo abelii</i>	USNM 143594	M	L	MS	M56426-101712	http://n2t.net/ark:/65665/3a893123e-021c-4f9b-ab42-4b4050332c24	—
<i>Pongo abelii</i>	USNM 143596	F	L	MS	M56423-101709	http://n2t.net/ark:/65665/3c26ea641-6662-42df-9b0d-a288ade0d69c	—
<i>Pongo pygmaeus</i>	AMNH 200900	F	L	AMNH	—	—	NextEngine
<i>Pongo pygmaeus</i>	USNM 142169	F	L	USNM	—	—	NextEngine
<i>Pongo pygmaeus</i>	USNM 145302	F	L	USNM	—	—	NextEngine
<i>Pongo pygmaeus</i>	USNM 153805	F	R	USNM	—	—	NextEngine
<i>Pongo pygmaeus</i>	USNM 153822	F	L	USNM	—	—	NextEngine
<i>Pongo pygmaeus</i>	ZMS 1982-0092	F	R	ZMS	—	—	μCT (BIR ACTIS)
<i>Pongo pygmaeus</i>	USNM 145301	M	L	USNM	—	—	NextEngine
<i>Pongo pygmaeus</i>	USNM 145305	M	L	USNM	—	—	NextEngine
<i>Pongo pygmaeus</i>	USNM 153823	M	L	USNM	—	—	NextEngine

<i>Pongo pygmaeus</i>	ZMS 1909-0801	M	L	ZMS	—	—	μCT (BIR ACTIS)
<i>Pongo pygmaeus</i>	ZMS 1966-0203	M	R	ZMS	—	—	μCT (BIR ACTIS)
<i>Pongo pygmaeus</i>	ZMB 87092	?	L	ZMB	—	—	μCT (BIR ACTIS)
<i>Symphalangus syndactylus</i>	AMNH 106583	F	L	AMNH	—	—	NextEngine
<i>Symphalangus syndactylus</i>	NMNH 271048	F	L	USNM	—	—	NextEngine
<i>Symphalangus syndactylus</i>	AMNH 106581	M	L	AMNH	—	—	NextEngine
<i>Symphalangus syndactylus</i>	PSU 105-1841	?	L	MS	M45351-82643	—	—
<i>Symphalangus syndactylus</i>	UWBM 58721-1	?	R	MS	M69298-125011	—	—
<i>Symphalangus syndactylus</i>	UWBM 82801-1	?	L	MS	M69299-125019	—	—
<i>Symphalangus syndactylus</i>	ZMB 38573	?	R	ZMB	—	—	μCT (BIR ACTIS)
<i>Symphalangus syndactylus</i>	ZMB 38587	F	L	ZMB	—	—	μCT (BIR ACTIS)

Abbreviations: F = female; M = male; ? = unknown sex; L = left; R = right; AMNH = American Museum of Natural History, New York, USA; CMNH = Cleveland Museum of Natural History, Cleveland, USA; MPI-EVA = Max Planck Institute for Evolutionary Anthropology, Leipzig, Germany; MS = MorphoSource.org; PCM = Powell-Cotton Museum, Birchington, UK; RMCA = Royal Museum for Central Africa, Tervuren, Belgium; SBU = Stony Brook University, New York, USA; USNM = Smithsonian National Museum of Natural History, Washington D.C., USA; ZMB = Museum für Naturkunde – Leibniz Institute for Evolution and Biodiversity Science, Berlin, Germany; ZMS = Zoologische Staatssammlung Munchen, Munich, Germany.

SOM Table S3

Landmark (L) and semilandmark (SL) protocol for KNM-BG 40021.^a

L/SL no.	Description
Fovea capitis	
L1	Most medial point on fovea capitis outline
L2	Most anterior point on fovea capitis outline
L3	Most lateral point on fovea capitis outline
SL1	Midpoint between L1 and L2 on fovea outline
SL2	Midpoint between L2 and L3 on fovea outline
Radial head	
L4	Most medial point on radial head outline
L5	Most anterior point on radial head outline
L6	Most lateral point on radial head outline
SL3	Midpoint between L4 and L5 on radial head outline
SL4	Midpoint between L5 and L6 on radial head outline
L7	Most medial point on distal articular expansion of the radial head
L8	Most anterior point on distal articular expansion of the radial head
L9	Most lateral point on distal articular expansion of the radial head
SL5	Midpoint between L7 and L8 on distal articular expansion of the radial head
SL6	Midpoint between L8 and L9 on distal articular expansion of the radial head

^a True landmarks (type II) and semilandmarks follow the descriptions of Bookstein (1997) and O'Higgins (2000).

SOM Table S4

Number of correctly classified specimens (and percentages within parentheses) by the bgPCA for extant taxa without cross-validation.

Taxon	Cercopithecines	Colobines	Hominids	Hylobatids	Platyrrhines
Cercopithecines	12 (75.0%)	0 (0%)	1 (6.3%)	0 (0%)	3 (18.8%)
Colobines	0 (0%)	6 (75.0%)	0 (0%)	0 (0%)	2 (25.0%)
Hominids	0 (0%)	0 (0%)	48 (81.4%)	9 (15.2%)	2 (3.4%)
Hylobatids	0 (0%)	0 (0%)	0 (0%)	14 (100%)	0 (0%)
Platyrrhines	1 (5.3%)	3 (15.8%)	2 (10.5%)	0 (0%)	13 (68.4%)

bgPCA = between-group principal component analysis.

SOM Table S5

Number of correctly classified specimens (and percentages within parentheses) by the bgPCA for extant taxa with cross-validation.

Taxon	Cercopithecines	Colobines	Hominids	Hylobatids	Platyrrhines
Cercopithecines	11 (68.7%)	1 (6.2%)	1 (6.25%)	0 (0%)	3 (18.7%)
Colobines	0 (0%)	6 (75,0%)	0 (0%)	0 (0%)	2 (25,0%)
Hominids	0 (0%)	0 (0%)	45 (76.3%)	11 (18.6%)	3 (5.1%)
Hylobatids	0 (0%)	0 (0%)	2 (14.3%)	12 (85.7%)	0 (0%)
Platyrrhines	2 (10.5%)	4 (21.0%)	3 (15.8%)	0 (0%)	10 (52.6%)

bgPCA = between-group principal component analysis.

SOM References

- Adams, D.C., Collyer, M.L. 2016. On the comparison of the strength of morphological integration across morphometric datasets. *Evolution* 70, 2623–2631.
- Adams, D.C., Collyer, M.L., Kaliontzopoulou, A., 2020. Geomorph: Software for geometric morphometric analyses. R package version 3.2.1. <https://cran.r-project.org/package=geomorph>.
- Arias-Martorell, J., Almécija, S., Urciuoli, A., Nakatsukasa, M., Moyà-Solà, S., Alba, D.M., 2021. A proximal radius of *Barberapithecus huerzeleri* from Castell de Barberà: Implications for locomotor diversity among pliopithecoids. *J. Hum. Evol.* 157, 103032.
- Blomberg, S.P., Garland, T., Ives, A.R., 2003. Testing for phylogenetic signal in comparative data: behavioral traits are more labile. *Evolution* 57, 717–745.
- Bookstein, F.L., 1997. Landmark methods for forms without landmarks: Localizing group differences in outline shape. *Med. Imaging Anal.* 1, 225–243.
- Freckleton, R.P., Harvey, P.H., Pagel, M., 2002. Phylogenetic analysis and comparative data: A test and review of evidence. *Am. Nat.* 160, 712–726.
- Le Gros Clark, W.E., Thomas, D.P., 1951. Associated jaws and limb bones of *Limnopithecus macinnesi*. *Fossil Mammals Afr.* 3, 1–27.
- O’Higgins, P., 2000. The study of morphological variation in the hominid fossil record: biology, landmarks and geometry. *J. Anat.* 197, 103–120.
- Pagel, M., 1999. Inferring the historical patterns of biological evolution. *Nature* 401, 877–884.
- Rose, M.D., Leakey, M.G., Leakey, R.E.F., Walker, A.C., 1992. Postcranial specimens of *Simiolus enjessi* and other primitive catarrhines from the early Miocene of Lake Turkana, Kenya. *J. Hum. Evol.* 22, 171–237.
- Rossie, J.B., Gutierrez, M., Goble, E., 2012. Fossil forelimbs of *Simiolus* from Moruorot, Kenya. *Am. J. Phys. Anthropol.* 147 (S54), 252.
- Senut, B., 1989. *Le Coude des Primates Hominoïdes. Anatomie, Fonction, Taxonomie, Évolution.* Éditions du Centre National de la Recherche Scientifique, Paris.
- Sherwood, R.J., Ward, R.J., Hill, A., Duren, D.L., Brown, B., Downs, W., 2002. Preliminary description of the *Equatorius africanus* partial skeleton KNM-TH 28860 from Kipsaramon, Tugen Hills, Baringo District, Kenya. *J. Hum. Evol.* 42, 63–73.
- Walker, A.C., Pickford, M., 1983. New postcranial fossils of *Proconsul africanus* and *Proconsul nyanzae*. In: Ciochon, R.L., Corruccini, R.S. (Eds.), *New Interpretations of Ape and Human Ancestry.* Plenum Press, New York, pp. 325–351.

- Ward, S., Brown, B., Hill, A., Kelley, J., Downs, W., 1999. *Equatorius*: A new hominoid genus from the middle Miocene of Kenya. *Science* 285, 1382–1386.
- Zapfe, H., 1958. The skeleton of *Pliopithecus (Epipliopithecus) vindobonensis* Zapfe and Hürzeler. *Am. J. Phys. Anthropol.* 16, 441–457.
- Zapfe, H., 1961. Die Primatenfunde aus der miozänen Spaltenfüllung von Neudorf an der March (Děvínská Nová Ves), Tschechoslowakei. *Schweizer. Palaeontol. Abh.* 78, 1–293.
- Zelditch, M. L., Swiderski, D. L., Sheets, H. D., 2012. *Geometric morphometrics for biologists: A primer*. New York, Academic Press.